The American Journal of Pathology, Vol. 193, No. 12, December 2023

ELSEVIER

The American Journal of PATHOLOGY

ajp.amjpathol.org

CELL INJURY, REPAIR, AGING, AND APOPTOSIS

Resolvin D2—G-Protein Coupled Receptor 18 Enhances Bone Marrow Function and Limits Steatosis and Hepatic Collagen Accumulation in Aging

Hannah Fitzgerald,* Jesse L. Bonin,† Sayeed Khan,* Maya Eid,* Sudeshna Sadhu,* Allison Rahtes,* Masharh Lipscomb,* Nirupam Biswas,† Christa Decker,* Melisande Nabage,* Ramon Bossardi Ramos,* Giesse Albeche Duarte,* Michael Marinello,* Anne Chen,‡ Hasan Basri Aydin,‡ Hebe Agustina Mena,§ Kurrim Gilliard,* Matthew Spite,§ C. Michael DiPersio,*¶ Alejandro P. Adam,* Katherine C. MacNamara,† and Gabrielle Fredman*

From the Departments of Molecular and Cellular Physiology, Immunology and Microbial Disease,† Pathology,‡ and Surgery,¶ Albany Medical College, Albany, New York; and the Department of Anesthesiology, Perioperative and Pain Medicine,§ Center for Experimental Therapeutics and Reperfusion Injury, Brigham and Women's Hospital and Harvard Medical School, Boston, Massachusetts*

Accepted for publication August 8, 2023.

Address correspondence to Gabrielle Fredman, Ph.D., Department of Molecular and Cellular Physiology, Albany Medical College, Albany, NY 12208; or Katherine C. MacNamara, Ph.D., Department of Immunology and Microbial Disease, Albany Medical College, Albany, NY 12208. E-mail: fredmag@amc.edu or macnamk@amc.edu.

Aging is associated with nonresolving inflammation and tissue dysfunction. Resolvin D2 (RvD2) is a proresolving ligand that acts through the G-protein—coupled receptor called GPR18. Unbiased RNA sequencing revealed increased *Gpr18* expression in macrophages from old mice, and in livers from elderly humans, which was associated with increased steatosis and fibrosis in middle-aged (MA) and old mice. MA mice that lacked GPR18 on myeloid cells had exacerbated steatosis and hepatic fibrosis, which was associated with a decline in $Mac2^+$ macrophages. Treatment of MA mice with RvD2 reduced steatosis and decreased hepatic fibrosis, correlating with increased $Mac2^+$ macrophages, increased monocyte-derived macrophages, and elevated numbers of monocytes in the liver, blood, and bone marrow. RvD2 acted directly on the bone marrow to increase monocyte-macrophage progenitors. A transplantation assay further demonstrated that bone marrow from old mice facilitated hepatic collagen accumulation in young mice. Transient RvD2 treatment to mice transplanted with bone marrow from old mice prevented hepatic collagen accumulation. Together, this study demonstrates that RvD2-GPR18 signaling controls steatosis and fibrosis and provides a mechanistic-based therapy for promoting liver repair in aging. *(Am J Pathol 2023, 193: 1953—1968; https://doi.org/10.1016/j.ajpath.2023.08.011)*

Aging is associated with chronic, nonresolving inflammation that can lead to tissue dysfunction.[1,2] Therefore, understanding cellular programs and factors that promote the resolution of inflammation during aging may inform the development of new strategies that can limit age-related organ decline. The resolution of inflammation is an active process that is governed by numerous factors, such as specialized proresolving lipid mediators (SPMs).[3] Recent studies suggest that nonresolving inflammation in aging, or inflammaging, may persist due to an impairment in inflammation-resolution programs and that treatment with SPMs, like resolvins, tempers exuberant inflammation and age-related tissue dysfunction.[2,4,5] However, little is known about SPM-initiated mechanisms that limit features of inflammaging.

SPMs, like Resolvin D2 (RvD2), promote a proresolving and proreparative phenotype in human macrophages and in young mice in the context of infection and injury.[6–10] RvD2 acts through its G-protein—coupled receptor, called GPR18, which is expressed on macrophages in both humans and mice.[8] RvD2 regulates phagocytosis, adhesion receptor expression, and cytokine production in phagocytes.[6–8] The RvD2-GPR18 signaling axis is not immunosuppressive, boosts host immunity in polymicrobial sepsis[7] and in both *Escherichia coli* and *Staphylococcus aureus*[6,8] infections in

Supported by NIH grants HL153019 (G.F.), HL170249 (G.F. and K.C.M), HL106173 (M.S.), R35GM131842 (K.C.M), and AR063778 (C.M.D.).

H.F. and J.L.B. contributed equally to this work.

https://doi.org/10.1016/j.ajpath.2023.08.011

mice, and promotes tissue repair and regeneration in young mice.[10] Thus, the RvD2-GPR18 axis tames inflammation, does not compromise host defense, and promotes tissue repair in specific contexts, yet how this pathway functions in aging is not known.

Inflammaging is associated with chronic activation of the innate immune system, characterized by elevated levels of circulating proinflammatory cytokines.[1,11] Despite heightened innate immune programs, elderly individuals have reduced host defenses, limited vaccine efficacy, an overall decline of tissue function, and poor organ transplant efficacy.[12,13] Therefore, understanding mechanisms to limit tissue decline and/or boost tissue repair without comprising host defense in elderly individuals is an unmet clinical need. Monocytes and macrophages are considered integral cell types in the etiology of inflammaging.[14] The aging milieu typically primes monocytes and macrophages toward a proinflammatory phenotype and, as such, macrophages in this context participate in propagating inflammation by secreting proinflammatory cytokines and lipid mediators.[15] How to reprogram monocytes and macrophages toward a more proresolving and proreparative phenotype is of considerable interest in aging.

A consequence of inflammaging is organ dysfunction. The liver, for example, is one of the largest solid organs in the body that regulates metabolism and immunity[16] and an organ where age significantly increases the risk of fibrosis.[17] Macrophages are the most abundant immune cell in the liver, where they play critical roles in inflammation, fibrosis, or fibrosis resolution.[18,19] Aging is associated with maladaptive structural and functional modifications in the liver. For example, blood volume in the liver decreases and the exchange of molecules becomes hampered due to the capillarization of liver sinusoids. Livers from elderly individuals are also associated with increased steatosis and collagen (fibrosis). Indeed, nonalcoholic fatty liver diseases (NAFLDs) and nonalcoholic steatohepatitis (NASH) mainly affect the middle-aged (MA) and elderly populations.[20,21] Therefore, understanding how to limit age-related hepatic fibrosis is of clinical interest.

Here, an unbiased screen revealed increased *Gpr18* expression in macrophages from old mice and in livers from elderly humans, which was associated with increased steatosis and fibrosis in MA and old mice. MA mice that lack GPR18 on myeloid cells had exacerbated steatosis and hepatic collagen accumulation, which was associated with a decline in monocytes. Treatment of MA mice with RvD2 reduced liver fat and collagen accumulation, correlating with increased monocyte-derived macrophages and elevated numbers of monocytes in the liver, blood, and bone marrow. RvD2 acted directly on the bone marrow to increase monocyte-macrophage progenitors. Indeed, bone marrow transplanted from old mice induced collagen accumulation in the liver of young mice, and transient RvD2 treatment limited the ability of marrow to drive this aging phenotype. Together, this study demonstrates that RvD2-GPR18 signaling controls age-related steatosis and fibrosis and provides a mechanistic-based therapy for promoting liver repair in aging.

Materials and Methods

Experimental Animals

All animal experiments were conducted in accordance with the Albany Medical College (Albany, NY) Institutional Animal Care and Use Committee guidelines for animal care and were approved by the Animal Research Facility at Albany Medical College. Male C57BL/6 young mice (aged 2 to 3 months), middle-aged mice (aged 11 to 12 months), old mice (aged 17 to 19 months), and C57BL/6-Tg(UBC-GFP)30Scha/J (UBC-EGFP) mice were purchased from The Jackson Laboratory (JAX; Bar Harbor, ME). Male C57BL/6.SJL mice (expressing the *Ptprc* a allele; CD45.1) were purchased from Taconic Biosciences (Germantown, NY). Mice were housed in the Albany Medical College Animal Research Facility and fed a standard rodent chow diet during the experiment. Mice were socially housed in standard cages at 22°C under a 12-hour light and 12-hour dark cycle.

Generation of a Humanized *GPR18* Floxed Mouse

Murine *Gpr18* was removed and replaced with human *GPR18* that was flanked with two loxp sites. The original mice contained a NeoSTOP cassette, which was removed on breeding with an FLPe mouse flippase [B6.129S4-*Gt(ROSA)26Sortm1(FLP1)Dym*/RainJ; stock number 009086; JAX]. Once the NeoSTOP was successfully removed, these mice were then backcrossed with C57BL6 mice. After successive backcrossing with C57BL6 mice, human *GPR18* was confirmed with genotyping and mRNA expression via real-time quantitative PCR (qPCR). These human GPR18 floxed mice are referred to in the text as fl/fl mice. These fl/fl mice were then crossed with a lysozyme Cre (LysM; JAX; stock number 004781) to remove human GPR18 in myeloid cells. Successive rounds of breeding occurred to ensure the loss of murine Gpr18 and the loss of human GPR18 on myeloid cells, referred to in the text as mKO (or myeloid knockout).

RvD2 Treatment

The 11-month−old male C57BL/6 mice were purchased from JAX. Mice were intraperitoneally injected with either vehicle [phosphate-buffered saline (PBS)] or 250 ng of RvD2 (Cayman Chemicals, Ann Arbor, MI; catalog number 10007279), for 7 days consecutively. The mice were sacrificed in the morning of day 8, and their body weight and complete blood cell count were measured, peritoneal cells were isolated by lavage, and liver was collected for endpoint analysis, as described below. Mice were sacrificed ad

libitum, and the livers were perfused with PBS through the portal vein.

Complete Blood Cell Count

Whole blood from mice was collected in 10% EDTA tubes. Complete blood cell count was measured immediately using an Element HT5 hematology analyzer (Heska, Loveland, CO).

RNA Sequencing

Male C57BL/6 young (aged 2 months) mice or old (aged 18 months) mice were purchased from JAX. Mice were then intraperitoneally injected with 200 μg of Zymosan A (Sigma, St. Louis, MO; catalog number Z4250) per mouse. After 72 hours, peritoneal cells were harvested by lavage and cultured overnight in complete Dulbecco's modified Eagle's medium (DMEM) containing L-cell media. The following day, unattached cells were washed with PBS, and mRNA was extracted from the attached macrophages with a Qiagen (Hilden, Germany) RNeasy Mini kit (catalog number 74106), according to the manufacturer's instructions. RNA sequencing was performed at The Forsyth Institute (Cambridge, MA). There were three mice in each group, and RNA from each mouse was sequenced in triplicate. The gene counts were normalized by rlog transformation and analyzed by the DeSeq2 pipeline. The analyzed DeSeq2 results were uploaded on the web-based application called iPathway Guide, and significantly up-regulated and down-regulated genes and pathways were identified. The log2 fold change threshold was >0.6, and the *P*-value threshold of <0.05 was applied. Moreover, the Gene Set Enrichment Analysis was performed using the default settings (*https://www.ncbi.nlm.nih.gov/geo/query/acc.cgi?acc=GSE236974*; accession number GSE236974).

Bone marrow and liver RNA sequencing: The microarray data of 23 aging human male and female livers were downloaded from the Gene Expression Omnibus database (*https://www.ncbi.nlm.nih.gov/geo; accession number GSE133815*). In addition, the GSE98249 data set (*https://www.ncbi.nlm.nih.gov/geo/query/acc.cgi?acc=GSE98249*) was downloaded with bulk RNA-sequencing data of six young and six aging $CD11b^+$ macrophages from murine bone marrow. The expression level of each gene was transformed into a log2 base before further analysis. Differential gene expression was analyzed using DESeq2 version 3.16,[22] in R studio software version 4.3.1 (*https://www.r-project.org*). Significance was defined as $P < 0.05$.

Liver Picrosirous Red Staining

Livers were perfused and isolated from each mouse, fixed in 4% paraformaldehyde, and embedded in optimal cutting temperature compound. Liver sections (10 μm thick) were cut with a Leica Biosystems (Wetzlar, Germany) cryostat and mounted onto glass slides. Liver sections were gradually dehydrated in xylene and ethanol and were stained by hematoxylin and eosin staining. Furthermore, collagen content in the liver was determined by picrosirius red staining, as per the manufacturer's instructions (Polysciences, Warrington, PA; catalog number 24901). After staining, sections were mounted with aqueous mounting media and were examined under the microscope (Olympus DP74, Tokyo, Japan). Alterations in histology between the three groups were assessed and quantified using ImageJ software version 1.53q (NIH, Bethesda, MD; *https://imagej.net/ij/index.html*, last accessed June 15, 2023).

Liver Immunofluorescence

Murine livers were perfused, isolated, and placed in 500 μL of 4% paraformaldehyde overnight at room temperature. The livers were then placed in 500 μL of 30% sucrose solution for 48 hours at 4°C, then embedded in optimal cutting temperature compound. Murine livers were sectioned into 10- to 12-μm cross-sections using a Leica Cryostat Machine (CM1860) and stored at −80°C. Liver sections were stained at 4°C with anti−collagen IV (Col-IV; EMD Millipore, Burlington, MA; catalog number 3607063), anti−galectin 3 (Mac-2; Cedarlane, Burlington, ON, Canada; catalog number CL8942AP), or anti−α-smooth muscle cell actin and anti−collagen 1 alpha 1 (Col1a1) (Cell Signaling Technology, Danvers, MA; catalog numbers 19245 and 72026, respectively). For these stains, an antigen retrieval method was added for optimal antibody binding and visualization. Briefly, frozen sections were first placed in a slide holder and under a ventilation hood to dry for 15 minutes. The sections were then submerged in 1× PBS to rehydrate for at least 5 minutes, followed by a conventional rehydration using sequential incubations with xylene, 100%, 95%, 70%, and 50% ethanol, and distilled H_20 each for 1 minute. The slides were then submerged into Antigen Retrieval Buffer (Antigen Unmasking Solution Citric Acid Based; catalog number H-3300; Vector Biolabs, Malvern, PA), and the entire unit was placed in a 100°C water bath for 15 minutes. The unit was then removed from the hot water bath and left at room temperature for a 30-minute cooling period. The sections were blocked with 1% bovine serum albumin (BSA) and 10% goat serum for 1 hour at 4°C, followed by washes in 1× Tris-buffered saline with 0.1% Tween (TBST) and 0.1% Tween buffer three times for 5 minutes each. Primary antibodies were added to the slides in 1% BSA overnight at 4°C. After 24 hours, slides were washed with 1× TBST and 0.1% Tween buffer three times for 5 minutes each. Secondary antibodies were added in 1% BSA for 2 hours at 4°C, followed by a PBS wash. Finally, the sections were counterstained with Hoechst to identify nuclei. The slides were visualized on a Leica SPE confocal microscope. The mean fluorescence intensity and cell count per visual field were determined through analysis using ImageJ software.

For the transplantation experiments, murine livers were isolated, flash frozen in liquid nitrogen, and then stored at −80°C. These livers were then sectioned into 10- to 12-μm cross-sections using a Leica Cryostat Machine (CM1860) and stored at −20°C. Liver sections were stained at 4°C

with anti−collagen IV (EMD Millipore; catalog number 3607063). Frozen sections were submerged in ice-cold 100% methanol for 10 minutes. The sections were washed with PBS and then immediately blocked with 1% BSA and 10% goat serum for 1 hour at 4°C. The sections were washed with PBS to remove the blocking reagent, and primary antibodies were added in 1% BSA overnight at 4°C. After 2 hours, slides were washed with PBS, and secondary antibodies were added in 1% BSA for 2 hours at 4°C. The sections were washed again and counterstained with Hoechst to identify nuclei. The slides were visualized on a Leica SPE confocal microscope.

Oil Red O Staining

Liver sections were fixed in 4% paraformaldehyde for 5 minutes and then washed with 60% isopropanol for a further 5 minutes. Next, liver sections were stained with freshly prepared oil red O (Sigma; catalog number O0625) staining solution for 30 minutes. Following incubation, they were washed with 60% isopropanol for 2 minutes and immediately rinsed in distilled water. Stained liver sections were mounted with Immumount (Thermo Fisher Scientific, Waltham, MA), and images were viewed on 20× objective lens using an Olympus DP74 microscope and Olympus DP2-BSW software. Oil red O−positive areas were quantified by threshold analysis using ImageJ software.

Triglyceride Assay

Livers were perfused, isolated, and immediately snap frozen in liquid nitrogen. Liver homogenates were subjected to triglyceride assay (Cell Biolabs, San Diego, CA; catalog number STA-396), according to the manufacturer's instructions.

Human Liver Autopsy Specimen

The institutional database at Albany Medical Center was searched for autopsy cases containing sampled liver, without known premortem liver disease and without a liver-related cause of death. The inclusion criteria for the three cohorts included the aforementioned criteria as well as the respective age range for each of the following two cohorts: young age cohort (aged 3 to 32 years) and middle-aged cohort (aged 35 to 54 years). This process resulted in 10 autopsy livers from the young age cohort (age range, 3 to 30 years; mean, 19 years; median, 19.5 years) and 11 autopsy livers from the middle-aged cohort (age range, 35 to 54 years; mean, 48 years; median, 49 years). The time frames of the autopsies from the cohorts are as follows: year 2015 to 2022 for the young age cohort, year 2019 to 2022 for the middle-aged cohort, and year 2020 to 2021 for the old age cohort. For the young age cohort, older archived cases were required to find a comparable number of cases, given that most hospital autopsies are from older patients. The available hematoxylin and eosin−stained slides originally collected at the time of the autopsy were pulled from the department archives and evaluated for the percentage of steatosis and the Non-Alcoholic Steatohepatitis Clinical Research Network (NASH-CRN) fibrosis score. The NASH-CRN fibrosis score[23] is used to evaluate fibrosis in the setting of known NAFLD. Although these autopsy patients did not have known NAFLD, because the authors are assessing the degree of steatosis and related fibrosis, this fibrosis scoring system was chosen as the most appropriate. The percentage of steatosis was quantified as the area percentage of liver occupied by macrovesicular fat globules visually assessed on the original hematoxylin and eosin−stained slides from the archived autopsy case. The NASH-CRN fibrosis score was assessed as follows: no fibrosis (score 0), perisinusoidal or portal fibrosis (score 1), perisinusoidal and portal fibrosis (score 2), bridging fibrosis (score 3), and cirrhosis (score 4).

Tissue Processing and Flow Cytometry

Perfused livers were isolated and processed by mincing with scissors, followed by enzymatic digestion. Liver mononuclear cells were isolated using the previously reported method of *in vitro* 0.05% collagenase incubation of liver specimens.[24−26] Briefly, the liver was perfused with 10 mL ice-cold PBS via the portal vein. Immediately after perfusion, the liver was removed and minced with scissors. Minced livers were centrifuged, and supernatant was removed. Homogenized livers were resuspended in 10 mL Hanks' balanced salt solution containing 0.05% collagenase (Type IV; Stem Cell Technology, Vancouver, BC, Canada; catalog number 07427), and the specimens were shaken for 20 minutes at 37°C. Digested liver tissue was centrifuged at 450 × *g* for 5 minutes at 4°C, and liver tissue was filtered through a 70-μm filter. Filtered liver tissue was resuspended in 10 mL 33% Percoll solution (Sigma-Aldrich, St. Louis, MO; catalog number P1644) and centrifuged at 600 × *g* for 20 minutes at room temperature (with brake set to 0). The supernatant was aspirated, and cell pellets were lysed with 200 μL of ACK buffer for 4 minutes at room temperature. After red blood cell lysis buffer, cells were washed twice and resuspended in Hanks' balanced salt solution containing fetal bovine serum and counted. Single-cell suspensions were plated and stained after incubation with Fc block using antibodies directed against myeloid cell markers [CD45.2 peridinchlorophyl-protein (PerCP) cyanin (Cy)5.5; F4/80 allophycocyanin (APC); Ly6C BV510; Ly6G BV605; CD115 phycoerythrin (PE); and CD11b PE Cy7] (Table 1). Data were acquired on a FACSymphony flow cytometer (BD Biosciences, Franklin Lakes, NJ) or a Northern Lights spectral flow cytometer (Cytek Biosciences, Fremont, CA) and analyzed using FlowJo software version 10.9.0 (TreeStar, Ashland, OR).

Bone marrow was flushed from both hind limbs and filtered through a 70-μm mesh filter. After red blood cell lysis (ACK lysis buffer), single-cell suspensions were plated and stained for flow cytometry. Cells were Fc blocked and then stained for hematopoietic stem and progenitor cells using antibodies

against lineage markers (CD3, CD11b, Gr-1, Ter-119, and CD45R) and hematopoietic stem and progenitor cell markers (c-Kit, Sca-1, CD150, CD48, and CD135) (Table 1). Cells were also stained with markers against myeloid cells (CD11b, Ly6C, Ly6G, CD115, F4/80, and CD115) (Table 1).

Liver qPCR

Minced mouse liver tissue was lysed using Trizol reagent (Thermo Fisher Scientific). RNA extraction was performed using chloroform and isopropanol precipitation, following the manufacturer's instructions. A total of 400 ng of RNA was reverse transcribed into cDNA using Primescript RT Master Mix (Clontech, Mountain View, CA) at 42°C, as directed by the manufacturer. The cDNA was diluted 10-fold in nuclease-free water. Each PCR contained 2 μL of cDNA. qPCR was conducted on a StepOnePlus instrument (Applied Biosystems, Waltham, MA) using 10 μL of SYBR Green–based iTaq supermix (Bio-Rad, Hercules, CA), 7.8 μL of water, and 2 pmol of primers (0.2 μL; Thermo Fisher Scientific). Fold induction was calculated using the $\Delta\Delta C_T$ method with hypoxanthine phosphoribosyltransferase 1 (HPRT) as the housekeeping gene.

RNAscope

Single-molecule RNA *in situ* detection (RNAscope; Advanced Cell Diagnostics, Newark, CA) was performed using the Multiplex Fluorescent kit version 2 (Advanced Cell Diagnostics; catalog number 323100) assay on 10-μm sections of freshly frozen liver tissue. Sections were fixed for 1 hour in 4% paraformaldehyde, dehydrated with ethanol in ascending concentrations, and pretreated with hydrogen peroxide for 10 minutes and protease IV for 20 minutes. Subsequently, sections were incubated at 40°C for 2 hours with the following probes for mRNA detection: adhesion G-protein coupled receptor-E1 (Adgre1; Advanced Cell Diagnostics; catalog number 460651-C2) and matrix metalloproteinase-9 (Mmp9; Advanced Cell Diagnostics; catalog number 315941-C3). The probe signal amplification was developed per the manufacturer's instructions for fresh frozen samples. Sections were counterstained with DAPI and mounted with Prolong Gold antifade reagent (Life Technologies Corp., Eugene, OR), then covered with glass coverslips and left to dry overnight in the dark. Sections were imaged on a fluorescence microscope (Eclipse 80i with Photometrics Cool Snap ES camera; Nikon, Tokyo, Japan). Quantification of *Mmp9* mRNA transcripts, which appear as puncta, was achieved by selecting a region of interest around individual Adgre1-positive macrophages and counting Mmp9 puncta inside individual regions of interest.

Colony-Forming Unit Assays

Bone marrow single-cell suspensions were first incubated for 30 minutes at 37°C in vehicle or RvD2. Cells were washed with 1× PBS and plated in methocellulose media (Methocult M3434; Stem Cell Technologies). Cells were plated (2 × 104 cells per 35-mm tissue culture dish) in duplicate, and plates were incubated for 7 to 8 days at 37°C in 5% CO_2. Plates were evaluated, and myeloid colonies were distinguished and counted under a light microscope.

Table 1 Antibody List

Marker	Species	Fluorophore	Clone	Company (catalog no.)
F4/80		APC	CI:A3-1	Abcam (Cambridge, UK) (AB105080)
Ly6C		Pacific Blue	HK1.5	BioLegend (San Diego, CA) (128013)
Ly6G		APC-Cy7	1A8	BioLegend (127623)
CD11b		PE-Cy7	M1/70	BioLegend (101216)
Gr-1		FITC	RB6-8C5	BioLegend (108406)
CD11b		FITC	M1/70	BioLegend (101206)
B220		FITC	RA3-6B2	BioLegend (103206)
Ter-119		FITC	TER-119	BioLegend (116206)
CD3		FITC	17A2	BioLegend (100204)
c-Kit		APC	2B8	BioLegend (105812)
CD48		Pacific Blue	HM48-1	BioLegend (103418)
CD41		BV510	MWReg30	BioLegend (133923)
CD150		BV711	TC15-12F1	BioLegend (115941)
CD135		PE	AF210	BioLegend (135306)
Sca-1		PE-Cy7	D7	BioLegend (108114)
CD115		PE	AFS98	BioLegend (135506)
CD45.2		BV711	104	BD Biosciences (563685)
Collagen IV	Rabbit		ATS2	EMD Millipore (AB756P)
Mac2	Rat		M3/38	Cedarlane Labs (8942AP)
COX2	Rabbit		D5H5	Cell Signaling Technology (12282S)
p-p38	Rabbit		T180/Y182	Cell Signaling Technology (9211S)
γH2AX	Rabbit		S139	Cell Signaling Technology (2577S)

APC, allophycocyanin; COX2, cyclooxygenase-2; Cy7, cyanin-7; FITC, fluorescein isothiocyanate; γH2AX, gamma histone H2AX; PE, phycoerythrin; p-p38, phosphorylated p38.

Bone Marrow Transplantation Experiments

Recipient 10-week−old C57BL/6.SJL male mice were treated with antibiotics [sulfamethoxazole and trimethoprim diluted in drinking water (200 mg/40 mg in 5 mL) for 10 days] before transplantation. Recipient mice were lethally irradiated with a total of 950 rads (split dose; 475 rads, 24 hours apart) and then reconstituted with a total of 5×10^5 total bone marrow cells. Mice were maintained on antibiotics for 15 days after transplantation and then placed on normal drinking water. Donor bone marrow was a 1:1 mixture of young whole bone marrow from UBC-EGFP mice and experimental bone marrow from donor young (7-week−old) or old (18-month−old) bone marrow treated with either vehicle (PBS) or RvD2. Donor bone marrow from young or old mice was incubated at 37°C for 30 minutes in vehicle or 1 nmol/L RvD2 and then washed with 1× PBS before transplant. Transplant recipients then received i.p. injections of either vehicle (PBS) or RvD2 (250 ng per mouse per day) for 5 days. Mice were allowed to recover and analyzed 4 months after transplantation. Livers were harvested from transplant recipients and analyzed to distinguish donor cells and myeloid populations (as described above).

Peritoneal Macrophage Immunofluorescence (*in Vitro*)

Peritoneal cells were isolated from young vehicle, old vehicle, or old RvD2 mice by lavage, and cultured overnight in complete DMEM containing L-cell media for macrophage differentiation. Peritoneal macrophages were fixed with 4% paraformaldehyde for 15 minutes, washed with 1× PBS, and permeabilized with 0.1% Titron X-100 for 15 minutes at room temperature. Fixed cells were blocked with blocking buffer (5% BSA in PBS + 0.1% Titron X-100 + 5% goat serum) and stained with rabbit anti-mouse phosphorylated p38 primary antibody at 1:200 dilution (Cell Signaling Technology; catalog number 9211), gamma histone H2AX (γH2AX; Cell Signaling Technology; 9211S), and cyclooxygenase-2 (COX2; Cell Signaling Technology; 12282S) overnight at 4°C. The next day, cells were washed with 1× PBS and incubated with goat anti-rabbit Alexa Fluor-594 secondary antibody (Invitrogen, Waltham, MA; A-11037) at 1:250 dilution for 2 hours at room temperature. Cell nuclei were stained with Hoechst (1 μg/mL) for 10 minutes, and images were acquired immediately on a Leica SPE confocal microscope. A total of six to seven different fields were acquired per well per antibody per mouse.

C-Reactive Protein, Insulin, and Col-IV Enzyme-Linked Immunosorbent Assays

Plasma was collected by spinning whole blood for 30 minutes, at 21,000 × *g* at 4°C. Plasma was assessed for C-reactive protein or Col-IV by enzyme-linked immunosorbent assay analysis according to the manufacturer [C-reactive protein (Thermo Fisher Scientific; catalog number EM20RB); and Col-IV (Novus Biologicals, Centennial, CO; catalog number NBP2-75865)]. Serum was collected and assessed for insulin by enzyme-linked immunosorbent assay (Crystal Chem, Elk Grove Village, IL; catalog number 90080) per manufacturer's instructions.

Phagocytosis Assay

Bone marrow−derived macrophages (BMDMs) were generated via flushing from femurs harvested from wild-type C57BL/6, fl/fl, and mKO mice. Using a 50-mL syringe, inject 5 mL of 10 mL DMEM, 10% fetal bovine serum, and 1% Pen-Strep L-cell media through both ends of the femur into a 50-mL tube. For each femur, inject 10 mL media in total. Once completed, there is 20 mL of sample in the 50-mL tube. Mix the 20 mL of the sample with an additional 20 mL of DMEM, 10% fetal bovine serum, and 1% PS media, to make a total of 40 mL, and mix it carefully by tipping the 50-mL tube. Pour the mixture through a 70-μm nylon cell strainer into a new 50-mL tube. Once completed, take four petri dishes and pipette 10 mL of the mixture. Ensure that the mixture is spread evenly across the petri dishes. Place the petri dishes in the incubator to allow the BMDMs to grow. At day 4 to 5, remove 5 mL of the medium from the petri dishes and replace it with 5 mL of fresh DMEM, 10% fetal bovine serum, and 1% Pen-Strep L-cell media.

BMDMs were then treated with vehicle or RvD2 (1 nmol/L) for 15 minutes, and subsequently opsonized fluorescent zymosan particles were added. After 30-minute incubation, fluorescent zymosan particles were washed off. Phagocytosis was assessed by a fluorescence plate reader by percentage increase of phagocytosis of RvD2.

Statistical Analysis

MA mice were randomly assigned to receive either vehicle or RvD2. Statistical differences between the *in vivo* groups were determined using the two-tailed *t*-test, *U*-test, or one-way analysis of variance or Kruskal-Wallis test with a Dunn post-test analysis using GraphPad Prism version 9.4.0 (Dotmatics, Boston, MA). All results are represented as means ± SEM. $P \leq 0.05$ was considered statistically significant. The figure legends have details regarding respective statistical tests.

Results

Gpr18 Expression Is Increased in Macrophages from Old Mice and in Livers from Old Humans

Macrophages are critical cellular players of both inflammation and resolution, and whether macrophages from old mice had distinct gene expression from young mice was of interest. Zymosan-elicited macrophages were harvested from young (2-month−old) and old (18-month−old) mice and subjected to bulk RNA sequencing. Principal component analysis revealed that peritoneal macrophages elicited

from old mice had distinct gene signatures compared with peritoneal macrophages from young mice (Figure 1A). Gene Set Enrichment Analysis revealed up-regulated pathways associated with inflammation (eg, COX2), mitogen-activated protein kinase signaling (eg, p38), and reactive oxygen species (Supplemental Figure S1A), which is consistent with other observations of age-related changes to macrophages.[19] GPR18 (which encodes the receptor for RvD2) was among the genes that were significantly up-regulated (Figure 1B). In addition, bone marrow–resident macrophages from old mice[27] had significantly increased *Gpr18* expression compared with those from young mice (Figure 1C). To test whether macrophages from old mice were responsive to RvD2, young or old mice were intraperitoneally injected with RvD2 (250 ng per mouse per day for 7 days), and peritoneal macrophages from young and old mice were collected by lavage. Macrophages from old mice had increased levels of COX-2 (Supplemental Figure S1B), phosphorylated p38 (Supplemental Figure S1C), and γH2AX (Supplemental Figure S1D) compared with macrophages from young mice, and RvD2 significantly decreased COX-2, phosphorylated p38, and γH2AX. These data demonstrate that macrophages from old mice have increased *Gpr18* expression and are responsive to RvD2 stimulation, suggesting that the RvD2-GPR18 axis, specifically in macrophages, may be a targetable signaling pathway to limit inflammaging.

In addition, differential gene expression analysis (iPathway Guide) suggested that several of the significantly up-regulated pathways in macrophages from aged mice were associated with inflammation, metabolism, and liver pathology, such as NAFLD (Figure 1D). Human livers from young (aged 21 to 45 years) and old (aged ≥69 years) individuals were examined for *GPR18* expression. Livers from old individuals had significantly increased expression of *GPR18* (Figure 1E). Collectively, these data suggest that elevated *GPR18* levels in macrophages from old mice and livers from old humans may yield important clues about new targetable approaches toward limiting inflammaging. Moreover, these data led to the next questions as to how macrophages and GPR18 signaling may play a role in age-related liver pathology.

Middle-Aged Mice Have Increased Liver Collagen and Fatty Deposits

The above results indicated an up-regulation in pathways associated with NAFLD. Therefore, lipid content was assessed in the liver from young (aged 2 to 3 month), MA (aged 11 to 12 month), and old (aged 17 to 19 month) mice fed a standard chow diet. Body weight significantly increased with age, as expected (young: 18.6 ± 1.7 g; MA: 32.7 ± 3.2 g; old: 42.3 ± 3.6 g). Lipid accumulation in the liver with oil red O staining and image analysis revealed a statistically significant increase in oil red O staining in MA and old livers compared with that in young livers (Figure 2, A and B). Hematoxylin and eosin staining revealed increased fatty deposits in MA and old livers (Figure 2C).

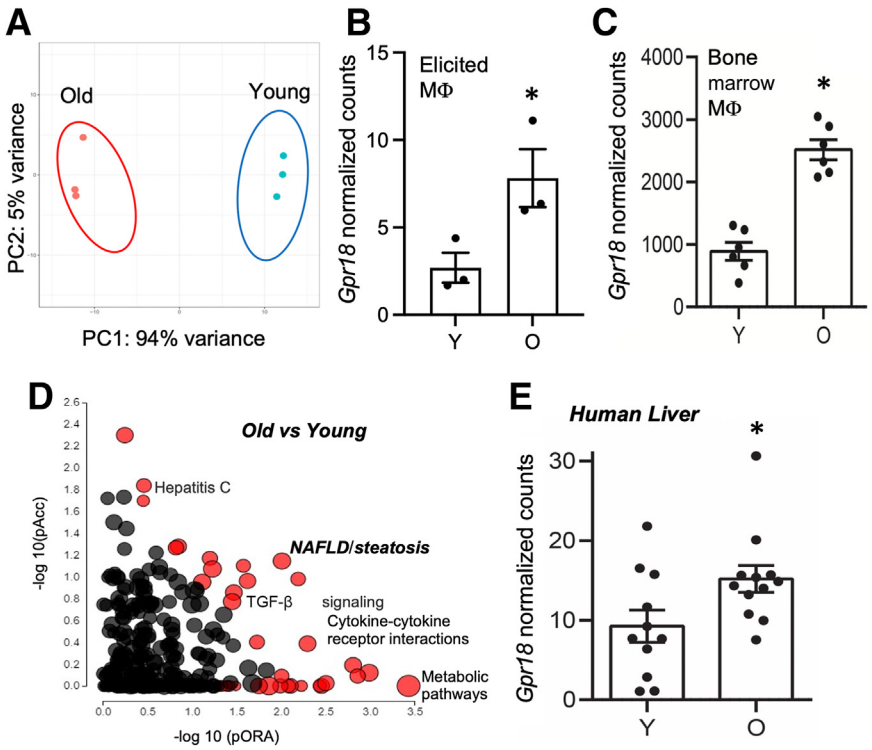

Figure 1 Differentially expressed genes and pathways in zymosan-elicited peritoneal macrophages from young (Y) and old (O) mice. RNA sequencing was performed on zymosan-elicited peritoneal macrophages (MΦ) from young (aged 2 months) or old (aged 18 months) mice, as described in *Materials and Methods*. **A:** Principal component (PC) analysis for the young or aged mice is shown. **B** and **C:** Normalized counts for *Gpr18* expression in zymosan-elicited macrophages (**B**) and murine bone marrow macrophages (**C**) are shown. **D:** iPathway Guide analysis shows biological pathways with significant perturbation accumulation (pAcc) and overrepresentation (pORA) in old compared with young mice. Significant pathways are shown in red, and nonsignificant pathways are shown in black. **E:** Normalized counts of GPR18 expression in human liver are shown. Each dot represents an individual mouse or human. Results are means ± SEM (**B**, **C**, and **E**). $^*P \leq 0.05$ (*t*-test). NAFLD, nonalcoholic fatty liver disease; TGF-β, transforming growth factor-β.

MA and old mice had significantly increased liver triglycerides in homogenized liver tissue compared with young mice (Figure 2D). These data demonstrate that accumulation of fat in liver occurs as early as middle age, which is consistent with the presence of NAFLD in middle age humans.[28]

Another histologic feature of liver aging, as with other key organs, is fibrosis. Livers were stained with picrosirius red for the identification of collagen networks, and images depict increased red color, which was significantly increased in the livers from MA and old mice (Figure 2, E and F) compared with young mice. Autopsy cases containing sampled liver, without known premortem liver disease or without a liver-related cause of death, were collected and assessed for fibrosis using the NASH-CRN scoring system.[23] The NASH-CRN fibrosis score was assessed as follows: no fibrosis (score 0), perisinusoidal or portal fibrosis (score 1), perisinusoidal and portal fibrosis (score 2), bridging fibrosis (score 3), and cirrhosis (score 4). Livers from middle-aged (aged 35 to 54 years) individuals had

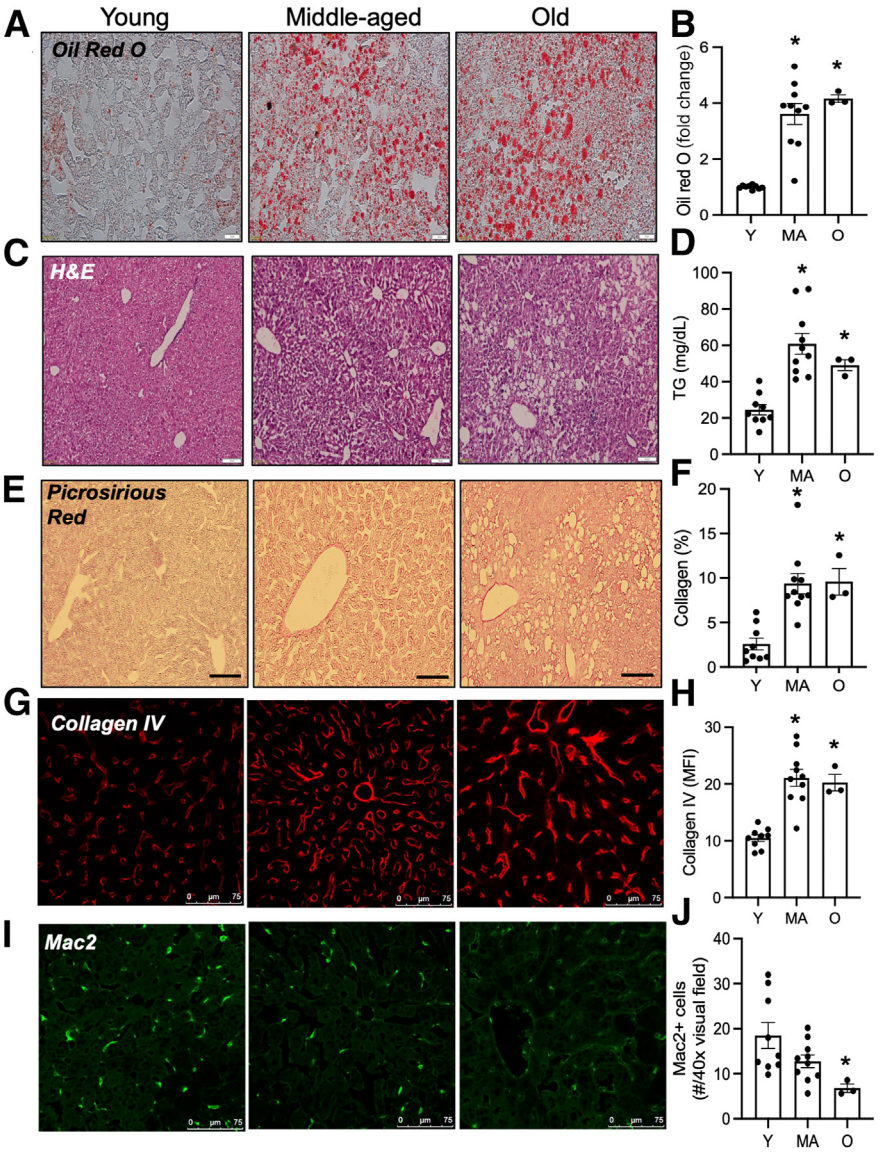

Figure 2 Middle-aged (MA) and old (O) mice have elevated steatosis and hepatic fibrosis compared with young (Y) mice. Livers from young (aged 2 months), middle-aged (aged 11 months), or old (aged 18 months) mice were harvested. **A:** Frozen liver sections were stained with oil red O, and lipid deposits are visualized as red. **B:** Quantification of oil red O was done by ImageJ software version 1.53q analysis. **C:** Liver sections were stained with hematoxylin and eosin (H&E), and representative images are shown. **D:** Liver homogenates were assessed for triglyceride (TG) content. **E** and **F:** Representative images and quantification of picrosirius red as percentage of red area per ×4 visual field. **A**–**C** and **E:** Images were acquired on an Olympus microscope, and the quantification was done by ImageJ software analysis. **G**–**J:** Representative images and quantification of liver sections that were immunostained with anti–collagen IV (Col-IV) antibody (red) or anti-Mac2 antibody (green; **I**). **G** and **I:** Images were acquired on a Leica confocal microscope and quantification of Col-IV mean fluorescence intensity (MFI; **H**) and the number of $Mac2^{+}$ cells/×40 visual field were enumerated with ImageJ software (**J**). Each dot represents an individual mouse. Results are means ± SEM (**B**, **D**, **F**, **H**, and **J**). *$P < 0.05$ (Kruskal-Wallis and Dunn post-test). Scale bars: 20 μm (**A**); 100 μm (**C** and **E**); 75 μm (**G** and **I**).

increased fibrosis scores, in the 3 to 4 range, compared with livers from young (aged 3 to 32 years) individuals (Supplemental Figure S2).

Liver fibrosis is also associated with accumulation of collagens I, III, and IV.[29] Col-IV is a fibrillar collagen that is a major extracellular matrix component of the basement membrane. Liver sinusoids are unique because they are lined by a fenestrated endothelium that lacks a basement membrane. Formation of perisinusoidal basement membranes beneath the endothelium is an integral feature of capillarization of sinusoids, which can proceed fatty liver and fibrosis, and thus may be an early marker of liver disease or can be suggestive of advanced liver fibrosis.[30] More importantly, increased capillarization is associated with fibrosis in livers from elderly individuals.[31] Livers immunostained with an anti−Col-IV antibody revealed increased Col-IV signal (Figure 2G). Quantification demonstrated a significant increase in Col-IV staining in MA and old mice compared with that in young mice (Figure 2H). Together, these data suggest that steatosis and mild hepatic fibrosis occur as early as middle age.

Macrophages can promote fibrogenesis and resolve fibrosis.[18] The next question was whether aging was associated with differences in macrophages in the liver. Mac2 (ie, galectin-3) staining, which identifies macrophages, decreased with age (Figure 2I). Although there was a trend for decreased Mac2$^+$ cells in MA mice, the decrease reached statistical significance in old mice (Figure 2J). Mac2-expressing macrophages are phagocytic[32] and, therefore, the loss of Mac2 expression in livers from aging mice may be indicative of a decline in phagocytic macrophages. The absolute frequency of liver macrophages, as measured by F4/80 staining of total liver cells and flow cytometric analysis, did not change with age (young: 7.9% ± 1.9%; MA: 8.2% ± 1.8%; old: 9% ± 2.9%), suggesting that the population of Mac2$^+$ macrophages decreased with age. Together, these data suggest an association between decreased Mac2$^+$ macrophages and increased steatosis and hepatic fibrosis in MA livers compared with young controls.

Myeloid Gpr18 Limits Fat and Collagen Accumulation in Livers of Aging Mice

Because aging is associated with impaired inflammation-resolution programs,[2,4] and because *Gpr18* expression was increased in macrophages from old mice and in livers from elderly humans, the next question was whether the above changes occurred due to impairments in GPR18 signaling. To evaluate the role of GPR18 in myeloid cells in age-associated liver pathology, a new mouse model was generated wherein a floxed human *GPR18* allele was inserted to the mouse genome, replacing the murine *Gpr18* gene (Supplemental Figure S3A). The human floxed *GPR18* gene (referred to as hGPR18 fl/fl or fl/fl) was crossed with a *LysM*-driven Cre line to generate myeloid-specific GPR18 knockout mice (hGPR18mKO or mKO). First, BMDMs from wild-type C57BL/6, fl/fl, and mKO mice were evaluated to determine expression levels of both murine and human GPR18. There was a significant loss of murine *Gpr18* by qPCR in BMDMs from both fl/fl and mKO mice (Supplemental Figure S3B), and human *GPR18* was primarily expressed in the fl/fl mice (Supplemental Figure S3C). To determine whether human GPR18 was functional in murine cells, an *in vitro* phagocytosis assay was performed. Briefly, BMDMs were treated with vehicle or RvD2 (1 nmol/L) for 15 minutes, after which opsonized fluorescent zymosan particles were added. After 30 minutes, the fluorescent zymosan particles were washed off and phagocytosis was assessed by a fluorescence plate reader. RvD2 enhanced phagocytosis in BMDMs from C57BL6 control mice and the fl/fl mice, suggesting that the human GPR18 was as functional as murine GPR18 in murine cells (Supplemental Figure S3D). More importantly, RvD2 did not increase phagocytosis in the mKO BMDMs, demonstrating that both murine and human GPR18 were successfully removed in macrophages and that RvD2's ability to enhance phagocytosis was dependent on GPR18.

Whether GPR18 signaling on myeloid cells impacts steatosis and hepatic fibrosis in MA mice was investigated next. Livers of female fl/fl and mKO mice aged 10 to 12 months were assessed for lipids, collagen, α-smooth muscle cell actin$^+$ cells, and Mac2$^+$ macrophages, as described above. First, both control fl/fl and mKO young cohorts showed little oil red O staining, as expected, whereas MA mKO had significantly more oil red O staining compared with that in fl/fl MA controls (Figure 3A). These observations support an increase in steatosis in MA that was more severe in the absence of GPR18 in myeloid cells. This was independent of body weight as no significant differences in body weight were observed between the groups (young fl/fl 19.9 g ± 0.91 versus young mKO 21.4 g ± 0.85 and MA fl/fl 33.8 g ± 5.2 versus MA mKO 35.9 g ± 4.0). The MA fl/fl mice exhibited a significant increase in Col1a1 compared with young fl/fl control (Figure 3B). The increase in Col1a1 was exacerbated by the loss of *GPR18* in MA mice (Figure 3B). Hepatic stellate cells expression α-smooth muscle cell actin, and the presence of these cells significantly increased in the mKO young and MA mice, compared with fl/fl young controls (Figure 3C). Together, these data demonstrate that loss of GPR18 on myeloid cells drives steatosis and hepatic collagen accumulation in MA mice, suggesting that GPR18 expression is important for limiting these age-associated liver pathologies.

Because there was a decreasing trend for Mac2$^+$ macrophages in livers from MA mice, the next question investigated was whether the loss of GPR18 on myeloid cells would impact these cells in the liver. Liver sections were stained with Mac2, as above. Mac2$^+$ cells significantly decreased with age in the fl/fl control mice, which was further reduced with the loss of myeloid *GPR18* (Figure 3D). Collectively, these data reveal a key role for

cell-autonomous RvD2-GPR18 signaling in myeloid cells in controlling age-related steatosis and hepatic fibrosis. Thus, targeting GPR18 could offer a novel therapeutic strategy.

Resolvin D2 Limits Age-Related Steatosis and Collagen Accumulation in the Liver

To address the possibility of targeting GPR18 therapeutically, MA mice were administered vehicle or RvD2 (250 ng per mouse, intraperitoneally) daily for 7 days. Mice were then sacrificed, and tissues were collected for analysis. First, there were significantly decreased liver triglyceride levels in RvD2-treated mice (Figure 4A), without a change in body weight (Supplemental Figure S4A), liver weight/body weight ratio (Supplemental Figure S4B), or circulating insulin (Supplemental Figure S4C) or plasma triglycerides (Supplemental Figure S4D). Livers were next subjected to qPCR analysis, to examine whether the decrease in liver triglycerides was also associated with changes in lipid metabolism genes. Indeed, RvD2 decreased the expression of acetyl-CoA carboxylase and stearoyl-CoA desaturase, but not fatty acid synthase expression compared with MA controls (Supplemental Figure S5).

Livers were sectioned and stained with picrosirious red, which revealed reduced collagen deposition. Quantification revealed a statistically significant decrease in picrosirius red staining in MA + RvD2 mice compared with that in MA vehicle controls (Figure 4B and Supplemental Figure S6A). Immunofluorescence of livers for Col-IV was also significantly decreased by RvD2 (Figure 4C and Supplemental Figure S6B). Circulating Col-IV is a marker of liver fibrosis in aged humans. Indeed, RvD2 significantly decreased circulating levels of Col-IV compared with MA controls (Supplemental Figure S4E). Because hepatic stellate cells make collagen (eg, Col1a1) in the liver and express α-smooth muscle cell actin, the next question was whether RvD2 limits α-smooth muscle cell actin^{+} cells in the liver. Indeed, RvD2 treatment to MA mice significantly decreased the number of α-smooth muscle cell actin cells compared with that in MA controls (Figure 4D and Supplemental Figure S6C). There was also a decreased trend in *Acta2* mRNA expression in whole livers from mice treated with RvD2 (Supplemental Figure S7A). RvD2 also decreased some features of inflammation, including circulating levels of C-reactive protein (Supplemental Figure S4F) and *Il1b* expression (Supplemental Figure S7B) in the liver of MA mice compared with young mice. Matrix metalloproteinases have been implicated in liver fibrosis and NASH, and RvD2 treatment significantly decreased the expression of *Mmp2* and *Mmp9* (Supplemental Figure S7, C and D) in livers from MA mice compared with controls. Since macrophage MMP9 plays important roles in fibrosis resolution of the liver, RNAscope analysis was used to determine macrophage expression of *Mmp9* mRNA *in situ*. There was a significant decrease in the number of *Mmp9* puncta (ie, transcripts) in the *Adgre1* (ie, F4/80)−expressing cells in the liver (Supplemental Figure S7E), suggesting that RvD2 treatment may impact liver macrophage phenotype in a

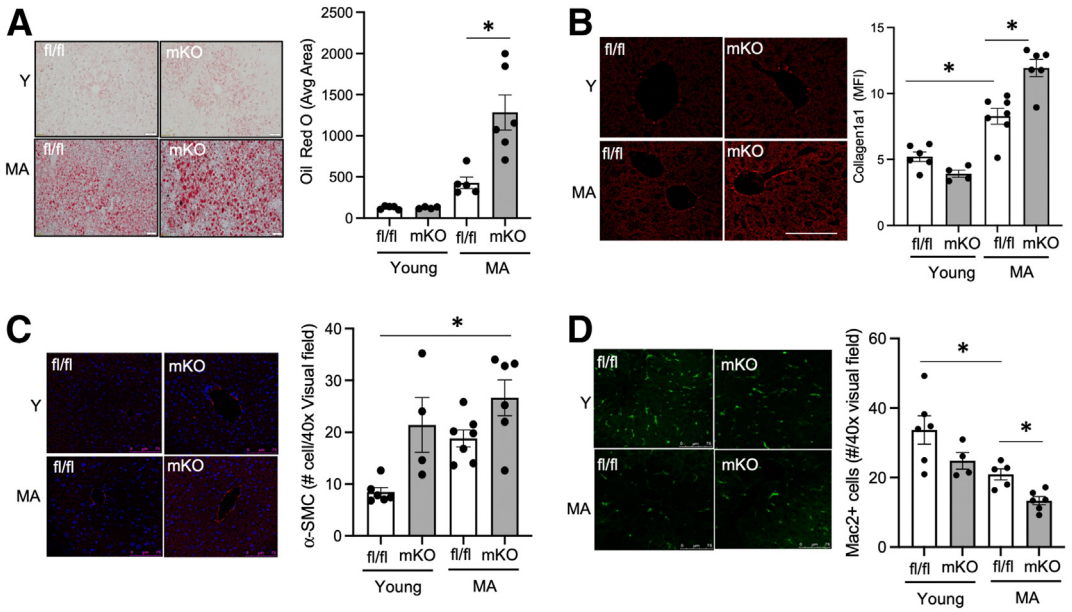

Figure 3 Middle-aged (MA) *Gpr18* myeloid knockout (mKO) mice have increased liver triglyceride, collagen, and α-smooth muscle cells (α-SMCs) and decreased macrophages compared with middle-aged fl/fl mice. Livers from young (Y; aged 4 months) and MA (aged 12 to 14 months) Grp18 fl/fl or mKO mice were evaluated. **A:** Frozen liver sections were stained with oil red O, and lipid deposits are visualized as red. Oil red O was quantified as in Figure 2. **B**–**D:** Paraffin-embedded livers from fl/fl and mKO mice were immunostained for Col1a1 (**B**), α-SMC (**C**), and Mac2 (**D**). Images were acquired on a Leica confocal microscope, and quantification of Col1a1 mean fluorescence intensity (MFI), α-SMC, and Mac2^{+} positive cells was done with ImageJ software version 1.53q. Each dot represents an individual mouse. Results are means ± SEM (**A**–**D**). *$P < 0.05$ (one-way analysis of variance with the Tukey multiple-comparison test). Scale bars: 20 μm (**A**); 75 μm (**B**–**D**).

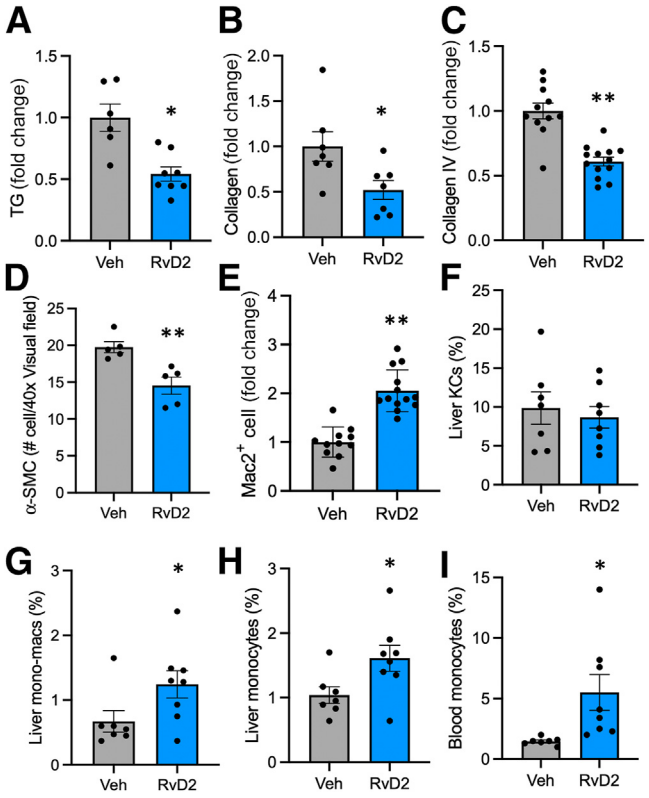

Figure 4 Resolvin D2 (RvD2) limits steatosis, reduces hepatic fibrosis, and increases Mac2$^+$ macrophages and monocytes in the livers from middle-aged (MA) mice. MA (aged 11 months) mice were treated with vehicle (Veh) or RvD2 (250 ng per mouse, intraperitoneally) for 7 days. Livers were harvested as in Figure 2. **A:** Liver homogenates were assessed for triglyceride (TG) content. **B:** Picrosirious red was analyzed by ImageJ software version 1.53q analysis and represented as fold change of Veh-treated mice. **C**–**E:** Collagen IV (**C**), α-smooth muscle cell (α-SMC; **D**), and Mac2 (**E**) acquired on a Leica confocal microscope, and quantification was done with ImageJ software. **F**–**H:** Liver was processed and analyzed by flow cytometry for Kupffer cells (KCs; Ly6G$^-$, CD11b^{lo}, F4/80^{hi}; **F**), monocyte-derived macrophages (mono-macs; Ly6G$^-$, CD11b$^+$, F4/80$^+$; **G**) and monocytes (Ly6G$^-$, CD11b$^+$, Ly6C^{hi}; **H**). **I:** Circulating monocytes were quantified by a Heska-HT5 analyzer. Each dot represents an individual mouse. Results are mean ± SEM (**A**–**I**). *$P < 0.05$, **$P < 0.01$ (*U*-test).

distinct manner compared with that in MA vehicle-treated controls. Together, these data demonstrate a significant improvement in age-related signatures of steatosis hepatic fibrosis and inflammation with just 1 week of RvD2 treatment.

Consistent with a potential role for macrophages in age-induced liver pathology, RvD2-treated MA mice had significantly increased Mac2$^+$ cells in the liver, as determined by immunofluorescence and confocal imaging (Figure 4E and Supplemental Figure S6D). RNAscope analysis revealed that the percentage of *Adgre1*-expressing cells was increased in the livers from RvD2-treated MA mice (Supplemental Figure S7F), again suggesting that macrophages were increased by RvD2 treatment. By flow cytometry, resident Kupffer cells were not changed between the two groups (Figure 4F and Supplemental Figure S8); however, RvD2 significantly increased monocyte-derived macrophages (CD11b^{hi} and F4/80$^+$) (Figure 4G and Supplemental Figure S8) and liver monocytes (Figure 4H).

The next question was whether monocytes in the liver increased due to systemic increases in circulating monocytes. Complete blood cell count analysis revealed that RvD2 treatment significantly increased the frequency of monocytes among circulating white blood cells in the blood (Figure 4I). Collectively, these data suggest that increased liver Mac2$^+$ macrophages, monocyte-derived macrophages, and monocytes in RvD2-treated mice correlate with decreases in steatosis and hepatic fibrosis in MA mice.

RvD2 Increases Monocytes in Bone Marrow and Promotes Monopoiesis

Monocytes are found in circulation, where they can be recruited into tissues to participate in replacement of macrophages. Monocytes were increased not only in livers from RvD2-treated MA mice, but also in the blood, which suggests a role for the bone marrow. MA mice treated with RvD2 exhibited a significant increase in frequency (Figure 5A) and number of bone marrow monocytes (Figure 5B). To determine whether RvD2 impacted hematopoietic progenitors, phenotypic hematopoietic stem and progenitor cells were analyzed by flow cytometry in MA mice with or without RvD2 treatment (Supplemental Figure S9). RvD2 induced an increase in the pool of lineage-negative cKit$^+$ Sca1$^+$ cells. However, within the lineage-negative cKit$^+$ Sca1$^+$ population, RvD2 reduced the frequencies of phenotypic hematopoietic stem cells and multipotent progenitors (MPPs) (Figure 5C). At the same time, RvD2 increased phenotypic, myeloid-biased MPPs (MPP$_{GM}$) within the lineage-negative cKit$^+$ Sca1$^+$ population (Figure 5C). Moreover, RvD2 significantly increased absolute frequencies (Figure 5D) and numbers of myeloid-committed MPP$_{GM}$ cells (Figure 5E) in the marrow. These data suggest that RvD2 treatment of MA mice induced an expansion of myeloid lineage–committed progenitors.

To examine the potential impact of RvD2 on functional myelopoiesis, bone marrow from MA mice was isolated and treated with whole bone marrow cells *ex vivo* with RvD2 (1 nmol/L), followed by Methocult assay to examine myeloid potential. Colony growth was analyzed after 1 week of culture, and myeloid colonies were enumerated (Figure 5F). There was a significant increase in macrophage colony-forming units, whereas no changes were observed in granulocyte colony-forming units or CFU–granulocyte/macrophage (Figure 5G), although a significant decrease in CFU–granulocyte/erythrocyte/monocyte/megakaryocyte was seen. Therefore, the increase in MPP$_{GM}$ *in vivo* and the striking increase in macrophage colony-forming units *in vitro* indicate that RvD2 increased monocyte and macrophage potential in MA mice. These data suggest that RvD2 acts directly on bone marrow cells to enhance monopoiesis and expedite differentiation of CFU–granulocyte/erythrocyte/monocyte/megakaryocyte

toward the monocyte lineage in MA mice. Collectively, these data reveal that RvD2 treatment results in a systemic increase in monocytes that correlates with decreased steatosis and hepatic fibrosis in the liver, suggesting that RvD2 may protect the liver by reprogramming hematopoietic function.

RvD2 Limits Age-Related Collagen Accumulation in the Liver in Part through Actions on Bone Marrow

Bone marrow chimeric mice were established to directly test the potential role of bone marrow function in driving the aging phenotype of the liver, and to test whether RvD2 could mitigate collagen accumulation via actions on bone marrow. Young recipient mice (CD45.1), aged 8 to 12 weeks, were lethally irradiated and reconstituted with congenic donor bone marrow from young (approximately 2 months) or old (17 months) mice, in combination with competitor donor bone marrow from young mice (Figure 6A). To determine whether RvD2 could mitigate the impacts of old bone marrow, donor bone marrow was treated with RvD2 *ex vivo* (as above) and then administered to transplant recipients for 1 week following transplantation. Vehicle-treated controls received the same numbers of injections during the week-long treatment. All mice were allowed to equilibrate for 4 months, where they received no further injections of RvD2 or vehicle before sacrifice and analysis of liver collagen.

Mice that received transplants of old bone marrow exhibited pronounced Col-IV (Figure 6, B and C) and Col1a1 (Figure 6D), relative to recipients of young bone marrow. This suggests that bone marrow–derived cells participate in age-associated liver collagen deposition. RvD2 treatment significantly reduced in Col-IV (Figure 6B) and Col1a1 (Figure 6D) staining in recipients that received old bone marrow. Therefore, treatment with RvD2 was able to reverse the collagen phenotype in recipients of old bone marrow. These data demonstrate that the age of the donor bone marrow contributed to amount of collagen in the liver and that even transient treatment with RvD2 was able to reverse this phenotype, correlating with increased monocytes.

Discussion

Herein, *Gpr18* expression was elevated in macrophages from old mice and livers from elderly humans, suggesting a link between increased *Gpr18* expression and inflammaging. Myeloid-specific RvD2-GPR18 signaling limited age-related steatosis and hepatic fibrosis. Mechanistically, RvD2 treatment of MA mice resulted in a systemic increase

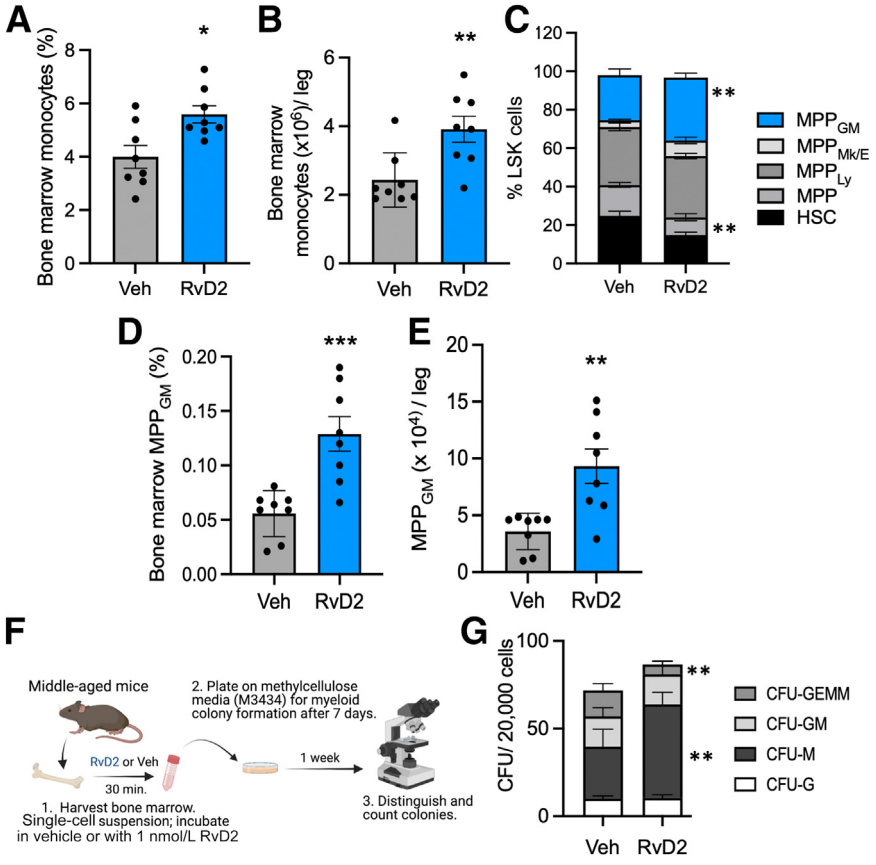

Figure 5 Resolvin D2 (RvD2) increases bone marrow monocytes and monocyte progenitors. Bone marrow was harvested, and monocytes were enumerated by flow cytometry. **A** and **B:** Monocyte ($CD11b^+$, $Ly6G^-$, $Ly6C^{hi}$) frequencies and numbers in middle-aged (MA) mice treated with vehicle (Veh) or RvD2 are shown. **C:** Frequencies of phenotypic hematopoietic stem and progenitor cells in bone marrow are shown as the percentage of each population among total lineage-negative, c-Kit^+, and Sca-1^+ cells (LSK). **D** and **E:** The absolute frequencies and number of granulocyte-macrophage multipotent progenitors (MPP_{GM}) are shown. **F** and **G:** Bone marrow was obtained from MA mice and incubated for 30 minutes with vehicle or RvD2 (1 nmol/L) and plated in Methocult media. After 7 days, colonies were counted. **G:** Colony-forming units (CFUs) are shown for macrophages (CFU-M), granulocytes (CFU-G), granulocyte/macrophage (CFU-GM), and granulocyte/erythrocyte/monocyte/megakaryocyte (CFU-GEMM) from MA bone marrow treated with Veh or RvD2. Results are from bone marrow. Each dot represents an individual mouse. Results are means ± SEM (**A**–**E** and **G**). $n = 4$ separate mice per treatment (**G**). $^*P < 0.05$, $^{**}P < 0.01$, $^{***}P < 0.001$ (U-test). HSC, hematopoietic stem cell. MPP_{Ly}, lymphocyte MPP; $MPP_{Mk/E}$, megakaryocyte/erythrocyte MPP.

in monocytes in the bone marrow, blood, and liver that correlated with decreased steatosis and hepatic fibrosis, suggesting that RvD2 may protect the liver by reprogramming hematopoietic function.

Aging is associated with increased chronic low levels of proinflammatory factors.[14] *Gpr18* expression was increased in macrophages from old mice, which was associated with increased gene sets for inflammation, mitogen-activated protein kinase signaling, and reactive oxygen species, to name a few. Proinflammatory ligands, like toll-like receptor 4 agonists (eg, lipopolysaccharide) and interferon-γ, increase *Gpr18* mRNA expression in murine macrophages,[33] which suggests that inflammation increases *Gpr18* expression. Conceptually, proinflammatory ligands, like prostaglandin E_2, are known to program resolution responses.[34] The current results suggest that another feed-back mechanism may include a complex of proinflammatory ligands and proresolving G-protein–coupled receptors. How *Gpr18* expression is regulated is not known, but the work presented herein and in the context of others suggests that proinflammatory factors and aging may drive its increased expression. Increased *Gpr18* expression in aging suggests it may be a compensatory response, and that GPR18 plays a protective role in the liver, bone marrow, and macrophages. By analogy, the triggering receptor on myeloid cells 2 is increased in NASH, but genetic deficiency of triggering receptor on myeloid cells 2 further worsens liver disease.[35,36] The data presented herein demonstrate that GPR18 is similarly increased during disease progression but plays a protective role because deficiency of GPR18 worsens disease. Moreover, the GPR18 receptor being upregulated in aging supports its therapeutic potential, as demonstrated herein.

The actions and mechanisms of RvD2 in aging were not known before this study. However, RvD1, another member of the D-series resolvin family, limits neutrophil infiltration into the peritoneum[2] and reduces neutrophils in the lungs after remote organ ischemia-reperfusion injury[4] in old animals. RvD1 treatment to aged mice reduces skeletal muscle inflammation and fibrosis, again suggesting a role for D-series resolvins in limiting inflammation and tissue injury in aging.[37] The mechanisms of actions of RvD1 in aging are not fully known. RvD1 binds and signals through distinct G-protein–coupled receptors, called formyl peptide receptor-2 (ALX/FPR2) (in mice and humans) and GPR32 (in humans), and a deeper exploration of these signaling axes in aging may yield important clue as to how neutrophils and other inflammatory factors may be regulated.

This study focused on an RvD2-GPR18 signaling axis. Briefly, RvD2 treatment limited steatosis and hepatic collagen that was associated with increased monocytes in the bone marrow, blood, and liver. Similarly, the SPM maresin 2 increased liver monocytes in diet-induced obesity young mice,[38] which was associated with reduced inflammation. Whether monocyte recruitment to the liver in the context of obesity or aging is a common function for SPMs remains to be explored. An increase in monocytes is associated with regression of atherosclerosis,[39] which is also associated with increased SPMs.[40] Indeed, monocytes are highly dynamic in their functions and can promote damage as well as repair. In acute liver injury in young mice, a subset of monocytes transition into a reparative phenotype that aid in liver wound repair.[41] Moreover, recruited monocytes can promote fibrosis resolution in mice, in part through the ability to promote phagocytosis.[42] Therefore, stimulating a phagocytic macrophage phenotype from monocyte-derived macrophages protects against liver fibrosis. Indeed, there is ample evidence suggesting a predominant role for macrophages in the progression of liver fibrosis or repair, which is contextual and may hinge on the

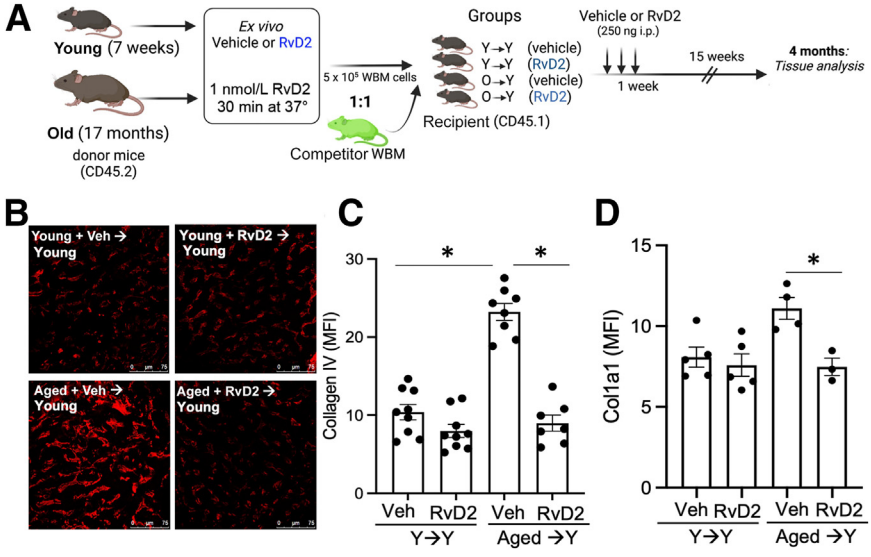

Figure 6 Resolvin D2 (RvD2) limits age-related hepatic collagen accumulation in part via changes in the bone marrow. **A:** Schematic of competitive bone marrow transplants where young mice received either young (Y) or old (O) donor bone marrow with or without RvD2 treatment. Recipient mice received injections of either vehicle (Veh) or RvD2 for 1 week, and mice were analyzed 4 months after transplant. **B:** Representative images and quantification of liver sections stained with anti–collagen IV (Col-IV) antibody shown in red. **C** and **D:** Images were acquired on a Leica confocal microscope, and quantification of Col-IV (**C**) or Col1a1 (**D**) mean fluorescence intensity (MFI) was done with ImageJ software version 1.53q. Each dot represents an individual mouse. Results are means ± SEM (**C** and **D**). $^*P < 0.05$ (one-way analysis of variance with Kruskal-Wallis and a Dunn post-test). Scale bar = 75 μm (**B**). WBM, whole bone marrow.

balance between tissue destructive and tissue-reparative MMPs.[18] How exactly RvD2 promotes the resolution of fibrosis is not known, but the data presented herein suggest that myeloid RvD2-GPR18 signaling is critical.

A recent study demonstrated that monocytes retain an inflammatory signature in the bone marrow during NAFLD progression.[43] This suggests that bone marrow monocytes can be programmed to retain phenotypic information when in target organs. Even newer data suggest a role for clonal hematopoiesis in chronic liver disease in humans, which also links the bone marrow to liver disease.[44] These data in the current context suggest that bone marrow may play a critical role in controlling liver disease and that RvD2 may imprint bone marrow to exert a proresolving function in the liver. From an endogenous perspective, RvD2 is produced within the bone marrow on ischemic inflammation[9] and so local production and signaling within the bone may be an additional mechanism for RvD2's protective actions. Indeed, in the current study, RvD2 acted directly on the bone marrow to functionally produce monocyte progenitors in middle age.

Aging is characterized by changes in blood production and immune responses that contribute to reduced vaccine efficacy, increased inflammation, and weakened host defenses seen in elderly individuals.[45] Well-described changes to hematopoiesis include cell production that favors myeloid cell output, including greater myeloid and megakaryocyte potential,[45] although stem cell function declines. The mechanisms driving these changes have been linked to both microenvironmental signals from the bone marrow niche[46] as well as cell-intrinsic molecular changes.[47–49] Signs of hematopoietic aging are evident in middle age,[50] which suggests that MA may be an appropriate time for intervention. Furthermore, the ability of old bone marrow to promote a fibrotic phenotype in livers from transplants in young mice demonstrates the important contribution of hematopoietic cells in age-induced hepatic fibrosis. More importantly, the transient treatment with RvD2 in the transplant experiments demonstrated the durability of its effects, as hepatic fibrosis was significantly reduced >3 months after RvD2 treatment.

A major proresolving feature of RvD2 was reduced steatosis and hepatic collagen accumulation in MA mice. SPMs limit several features of liver disease in young mice (as previously reviewed[51]). Some notable examples include that lipoxin A_4 limits diet-induced liver triglyceride and alanine transaminase levels,[52] suggesting a liver protective role in young mice fed a high-fat diet. Also, RvD1 limits steatosis and fibrosis in the methionine/chloline deficient diet NASH model.[53] Therefore, SPMs may be an intriguing therapeutic strategy in the context of liver diseases.

An important problem with anti-inflammatory treatment strategies is that they reduce host defense mechanisms. Indeed, blocking inflammation can lead to increased susceptibility of infections, which is especially critical in the elderly population, and so new ways to control inflammation without compromising host defense is an urgent clinical need. The RvD2-GPR18 signaling axis has been shown to boost host defense in mice. Indeed, evidence for the RvD2-GPR18 interaction *in vivo* came from studies of murine self-limited inflammation initiated by zymosan or *E. coli*. In mice with global deficiency of *Gpr18*, neutrophil infiltration during bacterial peritonitis is higher than that of wild-type littermate controls, leading to delayed resolution of acute inflammation.[8] This is associated with a defect in *E. coli* phagocytosis as well as macrophage efferocytosis. Administration of RvD2 expedites resolution and enhances efferocytosis when given at the peak of inflammation. These actions are not observed in GPR18-knockout mice, indicating that these resolution-enhancing roles of RvD2 are GPR18 dependent *in vivo*. Similarly, GPR18 is required for RvD2-dependent resolution of inflammation and enhancement of host defense in a distinct model of skin infection initiated by *S. aureus*.[8] Overall, this work suggests a new function for RvD2 in aging, which may prove to be an intriguing therapeutic in the context of age-related liver disease.

Author Contributions

G.F., H.F., J.L.B., S.S., S.K., H.A.M, and M.M. performed *in vivo* experiments; S.S. performed and analyzed the bulk RNA sequencing from young versus aged macrophages; R.B.R. and A.P.A. performed informatics analysis on human livers; H.F., C.D., and S.K. conducted and analyzed picrosirious red and oil red O staining of liver; M.L. conducted and analyzed the triglyceride assays; H.F., M.N., S.K., K.G., M.E., and A.R. conducted and analyzed liver immunofluorescence and enzyme-linked immunosorbent assays; G.A.D. and C.M.D. performed and analyzed RNAscope experiments; J.L.B. and N.B. conducted bone marrow and liver flow cytometry experiments; J.L.B. performed Methocult assays and performed and analyzed transplant experiments; A.C. and H.B.A. performed human liver pathology analyses; M.S., C.M.D., and A.R. supervised selected experiments; M.S., C.M.D., A.R., G.F., K.C.M., H.F., and J.L.B. wrote the manuscript; and K.C.M. and G.F. conceived the overall design of the experiments. The order of the first authors was determined on the basis of their contributions to the study.

Disclosure Statement

G.F. serves on a scientific advisory board for Esperion Therapeutics.

Supplemental Data

Supplemental material for this article can be found at *http://doi.org/10.1016/j.ajpath.2023.08.011*.

References

1. Shaw AC, Goldstein DR, Montgomery RR: Age-dependent dysregulation of innate immunity. Nat Rev Immunol 2013, 13:875–887
2. Arnardottir HH, Dalli J, Colas RA, Shinohara M, Serhan CN: Aging delays resolution of acute inflammation in mice: reprogramming the host response with novel nano-proresolving medicines. J Immunol 2014, 193:4235–4244
3. Serhan CN, Levy BD: Resolvins in inflammation: emergence of the pro-resolving superfamily of mediators. J Clin Invest 2018, 128: 2657–2669
4. Rymut NHJ, Sadhu S, Hosseini Z, Riley CO, Marinello M, Maloney J, MacNamara KC, Spite M, Fredman G: Resolvin D1 promotes efferocytosis in aging by limiting senescent cell-induced MerTK cleavage. FASEB J 2020, 34:597–609
5. Wong CK, Smith CA, Sakamoto K, Kaminski N, Koff JL, Goldstein DR: Aging impairs alveolar macrophage phagocytosis and increases influenza-induced mortality in mice. J Immunol 2017, 199: 1060–1068
6. Chiang N, de la Rosa X, Libreros S, Serhan CN: Novel resolvin D2 receptor axis in infectious inflammation. J Immunol 2017, 198: 842–851
7. Spite M, Norling LV, Summers L, Yang R, Cooper D, Petasis NA, Flower RJ, Perretti M, Serhan CN: Resolvin D2 is a potent regulator of leukocytes and controls microbial sepsis. Nature 2009, 461: 1287–1291
8. Chiang N, Dalli J, Colas RA, Serhan CN: Identification of resolvin D2 receptor mediating resolution of infections and organ protection. J Exp Med 2015, 212:1203–1217
9. Zhang MJ, Sansbury BE, Hellmann J, Baker JF, Guo L, Parmer CM, Prenner JC, Conklin DJ, Bhatnagar A, Creager MA, Spite M: Resolvin D2 enhances postischemic revascularization while resolving inflammation. Circulation 2016, 134:666–680
10. Giannakis N, Sansbury BE, Patsalos A, Hays TT, Riley CO, Han X, Spite M, Nagy L: Dynamic changes to lipid mediators support transitions among macrophage subtypes during muscle regeneration. Nat Immunol 2019, 20:626–636
11. Franceschi C, Garagnani P, Parini P, Giuliani C, Santoro A: Inflammaging: a new immune-metabolic viewpoint for age-related diseases. Nat Rev Endocrinol 2018, 14:576–590
12. Montecino-Rodriguez E, Berent-Maoz B, Dorshkind K: Causes, consequences, and reversal of immune system aging. J Clin Invest 2013, 123:958–965
13. Colvin MM, Smith CA, Tullius SG, Goldstein DR: Aging and the immune response to organ transplantation. J Clin Invest 2017, 127: 2523–2529
14. Hearps AC, Martin GE, Angelovich TA, Cheng WJ, Maisa A, Landay AL, Jaworowski A, Crowe SM: Aging is associated with chronic innate immune activation and dysregulation of monocyte phenotype and function. Aging Cell 2012, 11:867–875
15. De Maeyer RPH, Chambers ES: The impact of ageing on monocytes and macrophages. Immunol Lett 2021, 230:1–10
16. Bilzer M, Roggel F, Gerbes AL: Role of Kupffer cells in host defense and liver disease. Liver Int 2006, 26:1175–1186
17. Kim IH, Kisseleva T, Brenner DA: Aging and liver disease. Curr Opin Gastroenterol 2015, 31:184–191
18. Wynn TA, Vannella KM: Macrophages in tissue repair, regeneration, and fibrosis. Immunity 2016, 44:450–462
19. Stahl EC, Haschak MJ, Popovic B, Brown BN: Macrophages in the aging liver and age-related liver disease. Front Immunol 2018, 9:2795
20. Frith J, Day CP, Henderson E, Burt AD, Newton JL: Non-alcoholic fatty liver disease in older people. Gerontology 2009, 55:607–613
21. Sheedfar F, Di Biase S, Koonen D, Vinciguerra M: Liver diseases and aging: friends or foes? Aging Cell 2013, 12:950–954
22. Love MI, Huber W, Anders S: Moderated estimation of fold change and dispersion for RNA-seq data with DESeq2. Genome Biol 2014, 15: 550
23. Juluri R, Vuppalanchi R, Olson J, Unalp A, Van Natta ML, Cummings OW, Tonascia J, Chalasani N: Generalizability of the nonalcoholic steatohepatitis clinical research network histologic scoring system for nonalcoholic fatty liver disease. J Clin Gastroenterol 2011, 45:55–58
24. Kinoshita M, Uchida T, Sato A, Nakashima M, Nakashima H, Shono S, Habu Y, Miyazaki H, Hiroi S, Seki S: Characterization of two F4/80-positive Kupffer cell subsets by their function and phenotype in mice. J Hepatol 2010, 53:903–910
25. Liu Z, Gu Y, Shin A, Zhang S, Ginhoux F: Analysis of myeloid cells in mouse tissues with flow cytometry. STAR Protoc 2020, 1: 100029
26. Theurl I, Hilgendorf I, Nairz M, Tymoszuk P, Haschka D, Asshoff M, He S, Gerhardt LM, Holderried TA, Seifert M, Sopper S, Fenn AM, Anzai A, Rattik S, McAlpine C, Theurl M, Wieghofer P, Iwamoto Y, Weber GF, Harder NK, Chousterman BG, Arvedson TL, McKee M, Wang F, Lutz OM, Rezoagli E, Babitt JL, Berra L, Prinz M, Nahrendorf M, Weiss G, Weissleder R, Lin HY, Swirski FK: On-demand erythrocyte disposal and iron recycling requires transient macrophages in the liver. Nat Med 2016, 22:945–951
27. Frisch BJ, Hoffman CM, Latchney SE, LaMere MW, Myers J, Ashton J, Li AJ, Saunders J 2nd, Palis J, Perkins AS, McCabe A, Smith JN, McGrath KE, Rivera-Escalera F, McDavid A, Liesveld JL, Korshunov VA, Elliott MR, MacNamara KC, Becker MW, Calvi LM: Aged marrow macrophages expand platelet-biased hematopoietic stem cells via interleukin1B. JCI Insight 2019, 5:e124213
28. Estes C, Razavi H, Loomba R, Younossi Z, Sanyal AJ: Modeling the epidemic of nonalcoholic fatty liver disease demonstrates an exponential increase in burden of disease. Hepatology 2018, 67:123–133
29. Bataller R, Brenner DA: Liver fibrosis. J Clin Invest 2005, 115: 209–218
30. Hammoutene A, Rautou PE: Role of liver sinusoidal endothelial cells in non-alcoholic fatty liver disease. J Hepatol 2019, 70:1278–1291
31. Mak KM, Chen LL, Lee TF: Codistribution of collagen type IV and laminin in liver fibrosis of elderly cadavers: immunohistochemical marker of perisinusoidal basement membrane formation. Anat Rec (Hoboken) 2013, 296:953–964
32. Sano H, Hsu DK, Apgar JR, Yu L, Sharma BB, Kuwabara I, Izui S, Liu FT: Critical role of galectin-3 in phagocytosis by macrophages. J Clin Invest 2003, 112:389–397
33. Jablonski KA, Amici SA, Webb LM, Ruiz-Rosado Jde D, Popovich PG, Partida-Sanchez S, Guerau-de-Arellano M: Novel markers to delineate murine M1 and M2 macrophages. PLoS One 2015, 10:e0145342
34. Levy BD, Clish CB, Schmidt B, Gronert K, Serhan CN: Lipid mediator class switching during acute inflammation: signals in resolution. Nat Immunol 2001, 2:612–619
35. Hou J, Zhang J, Cui P, Zhou Y, Liu C, Wu X, Ji Y, Wang S, Cheng B, Ye H, Shu L, Zhang K, Wang D, Xu J, Shu Q, Colonna M, Fang X: TREM2 sustains macrophage-hepatocyte metabolic coordination in nonalcoholic fatty liver disease and sepsis. J Clin Invest 2021, 131:e135197
36. Hendrikx T, Porsch F, Kiss MG, Rajcic D, Papac-Milicevic N, Hoebinger C, Goederle L, Hladik A, Shaw LE, Horstmann H, Knapp S, Derdak S, Bilban M, Heintz L, Krawczyk M, Paternostro R, Trauner M, Farlik M, Wolf D, Binder CJ: Soluble TREM2 levels reflect the recruitment and expansion of TREM2(+) macrophages that localize to fibrotic areas and limit NASH. J Hepatol 2022, 77:1373–1385
37. Markworth JF, Brown LA, Lim E, Castor-Macias JA, Larouche J, Macpherson PCD, Davis C, Aguilar CA, Maddipati KR, Brooks SV: Metabolipidomic profiling reveals an age-related deficiency of

skeletal muscle pro-resolving mediators that contributes to maladaptive tissue remodeling. Aging Cell 2021, 20:e13393
38. Sugimoto S, Mena HA, Sansbury BE, Kobayashi S, Tsuji T, Wang CH, Yin X, Huang TL, Kusuyama J, Kodani SD, Darcy J, Profeta G, Pereira N, Tanzi RE, Zhang C, Serwold T, Kokkotou E, Goodyear LJ, Cypess AM, Leiria LO, Spite M, Tseng YH: Brown adipose tissue-derived MaR2 contributes to cold-induced resolution of inflammation. Nat Metab 2022, 4:775−790
39. Rahman K, Vengrenyuk Y, Ramsey SA, Vila NR, Girgis NM, Liu J, Gusarova V, Gromada J, Weinstock A, Moore KJ, Loke P, Fisher EA: Inflammatory Ly6Chi monocytes and their conversion to M2 macrophages drive atherosclerosis regression. J Clin Invest 2017, 127:2904−2915
40. Sharma M, Schlegel MP, Afonso MS, Brown EJ, Rahman K, Weinstock A, Sansbury BE, Corr EM, van Solingen C, Koelwyn GJ, Shanley LC, Beckett L, Peled D, Lafaille JJ, Spite M, Loke P, Fisher EA, Moore KJ: Regulatory T cells license macrophage pro-resolving functions during atherosclerosis regression. Circ Res 2020, 127:335−353
41. Dal-Secco D, Wang J, Zeng Z, Kolaczkowska E, Wong CH, Petri B, Ransohoff RM, Charo IF, Jenne CN, Kubes P: A dynamic spectrum of monocytes arising from the in situ reprogramming of CCR2+ monocytes at a site of sterile injury. J Exp Med 2015, 212:447−456
42. Ramachandran P, Pellicoro A, Vernon MA, Boulter L, Aucott RL, Ali A, Hartland SN, Snowdon VK, Cappon A, Gordon-Walker TT, Williams MJ, Dunbar DR, Manning JR, van Rooijen N, Fallowfield JA, Forbes SJ, Iredale JP: Differential Ly-6C expression identifies the recruited macrophage phenotype, which orchestrates the regression of murine liver fibrosis. Proc Natl Acad Sci U S A 2012, 109:E3186−E3195
43. Krenkel O, Hundertmark J, Abdallah AT, Kohlhepp M, Puengel T, Roth T, Branco DPP, Mossanen JC, Luedde T, Trautwein C, Costa IG, Tacke F: Myeloid cells in liver and bone marrow acquire a functionally distinct inflammatory phenotype during obesity-related steatohepatitis. Gut 2020, 69:551−563
44. Wong WJ, Emdin C, Bick AG, Zekavat SM, Niroula A, Pirruccello JP, et al: Clonal haematopoiesis and risk of chronic liver disease. Nature 2023, 616:747−754
45. Poscablo DM, Worthington AK, Smith-Berdan S, Forsberg EC: Megakaryocyte progenitor cell function is enhanced upon aging despite the functional decline of aged hematopoietic stem cells. Stem Cell Rep 2021, 16:1598−1613
46. Valletta S, Thomas A, Meng Y, Ren X, Drissen R, Sengul H, Di Genua C, Nerlov C: Micro-environmental sensing by bone marrow stroma identifies IL-6 and TGFbeta1 as regulators of hematopoietic ageing. Nat Commun 2020, 11:4075
47. Rundberg Nilsson A, Soneji S, Adolfsson S, Bryder D, Pronk CJ: Human and murine hematopoietic stem cell aging is associated with functional impairments and intrinsic megakaryocytic/erythroid bias. PLoS One 2016, 11:e0158369
48. Grover A, Sanjuan-Pla A, Thongjuea S, Carrelha J, Giustacchini A, Gambardella A, Macaulay I, Mancini E, Luis TC, Mead A, Jacobsen SE, Nerlov C: Single-cell RNA sequencing reveals molecular and functional platelet bias of aged haematopoietic stem cells. Nat Commun 2016, 7:11075
49. Florian MC, Nattamai KJ, Dorr K, Marka G, Uberle B, Vas V, Eckl C, Andra I, Schiemann M, Oostendorp RA, Scharffetter-Kochanek K, Kestler HA, Zheng Y, Geiger H: A canonical to non-canonical Wnt signalling switch in haematopoietic stem-cell ageing. Nature 2013, 503:392−396
50. Young K, Eudy E, Bell R, Loberg MA, Stearns T, Sharma D, Velten L, Haas S, Filippi MD, Trowbridge JJ: Decline in IGF1 in the bone marrow microenvironment initiates hematopoietic stem cell aging. Cell Stem Cell 2021, 28:1473−1482.e7
51. Claria J, Flores-Costa R, Duran-Guell M, Lopez-Vicario C: Pro-resolving lipid mediators and liver disease. Biochim Biophys Acta Mol Cell Biol Lipids 2021, 1866:159023
52. Borgeson E, Johnson AM, Lee YS, Till A, Syed GH, Ali-Shah ST, Guiry PJ, Dalli J, Colas RA, Serhan CN, Sharma K, Godson C: Lipoxin A4 attenuates obesity-induced adipose inflammation and associated liver and kidney disease. Cell Metab 2015, 22: 125−137
53. Li J, Deng X, Bai T, Wang S, Jiang Q, Xu K: Resolvin D1 mitigates non-alcoholic steatohepatitis by suppressing the TLR4-MyD88-mediated NF-kappaB and MAPK pathways and activating the Nrf2 pathway in mice. Int Immunopharmacol 2020, 88:106961